Calibration and Survey of AMANDA with the SPASE Detectors

The SPASE Collaboration and The AMANDA Collaboration

J. Ahrens[k] X. Bai[a,1] S.W. Barwick[j] R.C. Bay[i] T. Becka[k] K.-H. Becker[b] E. Bernardini[e] D. Bertrand[c] F. Binon[c] A. Biron[e] S. Böser[e] O. Botner[n] A. Bouchta[e,2] O. Bouhali[c] T. Burgess[o] S. Carius[f] T. Castermans[d] D. Chirkin[i] J. Conrad[n] J. Cooley[ℓ] D.F. Cowen[h] A. Davour[n] C. De Clercq[p] T. DeYoung[ℓ,3] P. Desiati[ℓ] J.-P. Dewulf[c] E. Dickinson[s,1] P. Doksus[ℓ] P. Ekström[o] R. Engel[a,8] P. Evenson[a,1] T. Feser[k] T.K. Gaisser[a,1] R. Ganugapati[ℓ] M. Gaug[e] H. Geenen[b] L. Gerhardt[j] A. Goldschmidt[g] A. Hallgren[n] F. Halzen[ℓ] K. Hanson[ℓ] R. Hardtke[ℓ] T. Hauschildt[e] M. Hellwig[k] P. Herquet[d] G.C. Hill[ℓ] J.A. Hinton[s,1] B. Hughey[ℓ] P.O. Hulth[o] K. Hultqvist[o] S. Hundertmark[o] J. Jacobsen[g] A. Karle[ℓ] J. Kim[j] L. Köpke[k] M. Kowalski[e] K. Kuehn[j] J.I. Lamoureux[g] H. Leich[e] M. Leuthold[e] P. Lindahl[f] I. Liubarsky[r] J. Lloyd-Evans[s,1] J. Madsen[m] K. Mandli[ℓ] P. Marciniewski[n] D. Martello[a,7,1] H.S. Matis[g] C.P. McParland[g] T. Messarius[b] T.C. Miller[a,4,1] Y. Minaeva[o] P. Miočinović[i] P.C. Mock[j,5] R. Morse[ℓ] T. Neunhöffer[k] P. Niessen[p] D.R. Nygren[g] H. Ögelman[ℓ] Ph. Olbrechts[p] C. Pérez de los Heros[o] A.C. Pohl[o] R. Porrata[j,6] P.B. Price[i] G.T. Przybylski[g] K. Rawlins[ℓ] E. Resconi[e] W. Rhode[b] M. Ribordy[e] S. Richter[ℓ] K. Rochester[s,1] J. Rodríguez Martino[o] P. Romenesko[ℓ] D. Ross[j] H.-G. Sander[k] T. Schmidt[e] K. Schinarakis[b] S. Schlenstedt[e] D. Schneider[ℓ] R. Schwarz[ℓ] A. Silvestri[j] M. Solarz[i] G.M. Spiczak[m,1] C. Spiering[e] M. Stamatikos[ℓ] T. Stanev[a,1] D. Steele[ℓ] P. Steffen[e] R.G. Stokstad[g] K.-H. Sulanke[e] I. Taboada[q] S. Tilav[a,1] C. Walck[o] W. Wagner[b] Y.-R. Wang[ℓ] A.A. Watson[s,1] C. Weinheimer[k] C.H. Wiebusch[e,2] C. Wiedemann[o] R. Wischnewski[e] H. Wissing[e] K. Woschnagg[i] W. Wu[j] G. Yodh[j] S. Young[j]

[a] *Bartol Research Institute, University of Delaware, Newark, DE 19716, USA*

[b] *Fachbereich 8 Physik, BUGH Wuppertal, D-42097 Wuppertal, Germany*

[c] *Université Libre de Bruxelles, Science Faculty CP230, Boulevard du Triomphe, B-1050 Brussels, Belgium*

[d] *Université de Mons-Hainaut, 19 Avenue Maistriau 7000, Mons, Belgium*

[e] *DESY-Zeuthen, D-15735 Zeuthen, Germany*

[f] *Dept. of Technology, Kalmar University, S-39182 Kalmar, Sweden*

[g] *Lawrence Berkeley National Laboratory, Berkeley, CA 94720, USA*

[h] *Dept. of Physics, Pennsylvania State University, University Park, PA 16802, USA*

[i] *Dept. of Physics, University of California, Berkeley, CA 94720, USA*

[j] *Dept. of Physics and Astronomy, University of California, Irvine, CA 92697, USA*

[k] *Institute of Physics, University of Mainz, Staudinger Weg 7, D-55099 Mainz, Germany*

[ℓ] *Dept. of Physics, University of Wisconsin, Madison, WI 53706, USA*

[m] *Physics Dept., University of Wisconsin, River Falls, WI 54022, USA*

[n] *Division of High Energy Physics, Uppsala University, S-75121 Uppsala, Sweden*

[o] *Dept. of Physics, Stockholm University, SCFAB, SE-10691 Stockholm, Sweden*

[p] *Vrije Universiteit Brussel, Dienst ELEM, B-1050 Brussel, Belgium*

[q] *Departamento de Física, Universidad Simón Bolívar, Apdo. Postal 89000, Caracas, Venezuela*

[r] *Imperial College, London*

[s] *Univerity of Leeds, Leeds, UK*

Abstract

We report on the analysis of air showers observed in coincidence by the Antarctic Muon And Neutrino Detector Array (AMANDA-B10) and the South Pole Air Shower Experiment (SPASE-1 and SPASE-2). We discuss the use of coincident events for calibration and survey of the deep AMANDA detector as well as the response of AMANDA to muon bundles. This analysis uses data taken during 1997 when both SPASE-1 and SPASE-2 were in operation to provide a stereo view of AMANDA.

[1] SPASE Collaboration

[2] Present address: CERN, CH-1211, Geneve 23, Switzerland

[3] Present address: Santa Cruz Institute for Particle Physics, University of California, Santa Cruz, CA 95064, USA

[4] Present address: Johns Hopkins University, Applied Physics Laboratory, Laurel, MD 20723, USA

[5] Present address: Optical Networks Research, JDS Uniphase, 100 Willowbrook Rd., Freehold, NJ 07728-2879, USA

[6] Present address: L-174, Lawrence Livermore National Laboratory, 7000 East Ave., Livermore, CA 94550, USA

[7] Present address: Dipt. di Fisica & INFN, Lecce, Italy

[8] Present address: Forschungszentrum Karlsruhe, Institut fur Kernphysik, Postfach 3640, 76021 Karlsruhe, Germany

1 Introduction

One of the advantages of a neutrino telescope in ice is the possibility of an air shower array on the surface to make coincidence measurements with the deep detector. The presence of SPASE on the surface provides a set of externally tagged muon bundles that can be measured by AMANDA. Such measurements allow a study of the response of AMANDA that is complementary to studies of the deep detector with atmospheric muons and neutrinos, internal calibration sources and Monte Carlo simulations. In particular, the surface array makes possible an independent check of the angular resolution of the deep detector. In addition it makes possible a muon survey of AMANDA optical module (OM) locations and ice properties that complements internal assessments.

Measurements of the muon bundles under 1500 m of ice in coincidence with showers at the surface also allows a novel study of the primary cosmic rays in the region of the knee of the cosmic-ray spectrum. In this paper we describe the calibration and survey of AMANDA with SPASE. In the process we study the response of AMANDA to muon bundles. Such measurements form the basis of the composition study, which is the subject of a separate paper [1].

1.1 Description of the surface arrays

There have been two South Pole Air Shower Experiments. SPASE-1 [2–4] was an array of 16 detectors, each 1 m^2 of scintillator, at 14 locations on a 30 m triangular grid. The array operated for ten years from the end of 1987 to the end of 1997. SPASE-2 [5] is an array of 120 modules grouped into 30 stations on a 30 m triangular grid. Each module contains a scintillator of 0.2 m^2. The enclosed area of SPASE-1 was approximately 6000 m^2 while that of SPASE-2 is 16,000 m^2. SPASE-2 began full operation at the beginning of 1996. AMANDA was deployed in stages; the 10-string array (AMANDA-B10) began operation in 1997 [6]. For the purpose of studying the response of AMANDA, 1997 is particularly important because of the unique opportunity to view AMANDA in stereo, from two different directions and at two zenith angles (27° for SPASE-1 and 12° for SPASE-2). In addition, the GASP air Cherenkov telescope [7] was also operating the same year and providing tagged coincidence events. We therefore concentrate in this paper on coincident data collected in 1997. Figure 1 shows a plan view of the physical configuration of the four detectors in 1997.

The pointing and angular resolution of SPASE-1 were measured with a pair of small atmospheric Cherenkov telescopes [9]. Each telescope consisted of a Fresnel lens with an aperture stop and a photomultiplier. The zenith and az-

imuth of the telescopes were measured with a lunar transit, using a flat mirror to reflect the image of the moon into the telescope aperture. Then cosmic-ray showers detected by both SPASE-1 and the Cherenkov telescopes were used to determine the the absolute pointing of the air shower array to $\pm 0.2^\circ$ in zenith and $\pm 0.5^\circ$ in azimuth. In addition, the coincident events were used to make a direct determination of the angular resolution of the air shower array as a function of shower size. This confirmed indirect determinations of angular resolution made by Monte Carlo simulations and by the sub-array method [2,5]. Absolute orientation of SPASE-2 was determined by conventional surveying techniques and its angular resolution by use of the indirect methods proven by SPASE-1.

The accuracy with which the surface arrays determine the directions of air showers increases from 3° at threshold to 1.5° for the larger showers used here to study angular resolution of AMANDA. The angular resolution as a function of shower size is shown explicitly in Fig. 7 of Ref. [5] as the half-angle of a cone that contains 63% of the events. This definition is appropriate for a two-dimensional Gaussian distribution. The rms error in location of shower cores decreases from 8 m at threshold to <5 m for the higher energy showers (Fig. 6 of Ref. [5]).

In addition to the air shower arrays, the GASP telescope [7] was also operating in the year 1997. GASP consisted of 10 mirrors, each viewed by 2 photomultiplier tubes, one pointing on-source and the other pointing 2.7deg off-source. In this run [8] the "source" was opposite the direction to the center of the instrumented portion of AMANDA-B10. The off-source direction was chosen to select events pointed toward the top of the instrumented volume. The GASP instrument had an optical angular acceptance of 0.5 degrees, an angular resolution of about one degree for cosmic-ray showers, with an energy threshold of approximately 1-2 TeV.

1.2 Description of AMANDA

The evolution and operation of the AMANDA detector are described in Ref. [6]. In this paper we concentrate on data obtained with AMANDA-B10, which consists of 10 vertical strings of detectors located as shown in the plan view of Fig. 1. Each string is instrumented with optical modules (OMs) at assigned depths between 1.5 and 2 km in clear Antarctic ice.

Altogether there are 302 optical sensors in AMANDA-B10, forming an instrumented cylinder of ice approximately 500 meters high and 120 meters in diameter. A line from the center of AMANDA-B10 to the center of SPASE-2 has a zenith angle of 12°. The corresponding angle to SPASE-1 is 27°. The

combination of a surface array of area A_s with the array deep in the ice constitutes a three-dimensional cosmic-ray detector with an acceptance of

$$\mathcal{A} \approx \frac{A_s \cos\theta \times A_{s-B10}}{d^2} = \Delta\Omega \times A_{s-B10}, \quad (1)$$

where A_{s-B10} is the projected area of AMANDA-B10 viewed at a zenith angle θ from the surface array and d is the distance between the centers of the two detectors. The solid angles of the acceptance cones are small, $\Delta\Omega_1 \approx 0.0015$ sr and $\Delta\Omega_2 \approx 0.005$ sr for SPASE-1/AMANDA-B10 and SPASE-2/AMANDA-B10 respectively. Given the dimensions listed above, $\mathcal{A}_1 \approx 50\,\mathrm{m}^2$ sr and $\mathcal{A}_2 \approx 100\,\mathrm{m}^2$ sr. Coincidence rates can be estimated by multiplying the acceptance with the flux of cosmic rays with energy above the threshold of each array. With thresholds for full efficiency of approximately 200 TeV, the coincidence rate is around 10^{-3} Hz for SPASE-2-AMANDA-B10.

1.3 Shower phenomenology in SPASE and AMANDA

A shower initiated by a high-energy primary cosmic-ray nucleus consists of a disk of relativistic secondary particles (mostly electrons and positrons with $E < 100$ MeV) propagating through the atmosphere at nearly the speed of light. The shower direction is reconstructed from the arrival times of the shower front at the detectors. A measure of the primary energy is given by the density of charged particles measured at a nominal perpendicular distance from the shower core. The nominal core distance used for the SPASE arrays is 30 m, and the particle density in units of vertical equivalent muons per m^2 at 30 m is denoted $S(30)$. It is also possible to use assumed or measured lateral distributions to obtain a fitted shower size. The relation between $S(30)$ and primary energy for simulated protons and iron primaries with $E > 100$ TeV and $\theta < 32°$ is shown in Fig. 2. Note that, as a consequence of fluctuations on a steep spectrum, average energy as a function of $S(30)$ is not the inverse of average $S(30)$ as a function of energy. Fluctuations are especially important near threshold. The upper panels of the figure illustrate how the reconstruction efficiency falls off in the threshold region.

To relate measured quantities to physical properties of the showers as in Fig. 2, we use a Monte Carlo simulation. Showers are generated with energies from 100 TeV to 100 PeV using a modified version of MOCCA [10] calling the QGSJET98 [11] hadronic interaction model. We use MOCCA for consistency with previous analysis of the SPASE/VULCAN data [12]. It has been updated to include separate treatment of kaons and consistent treatment of interactions of primary nuclei. The hadronic event generator QGSJET98 is generally considered to give the best representation of hadronic interactions in this energy

region [13]. High energy muons are propagated through the ice to the depth of AMANDA-B10 using MUDEDX [14] to make a stochastic calculation of muon energy losses. The response of AMANDA to light radiated by the muons is evaluated by the program AMASIM [15]. This program uses pre-calculated tables to simulate the arrival times and amplitudes of photo-electrons at the anodes of the photomultipliers. AMASIM then uses parameters of the hardware to generate a realistic response of the detector to the muons.

For an array of $0.8\,\mathrm{m}^2$ detectors on a 30 meter triangular grid, the threshold corresponds to showers with a density $S(30) \approx 1$. For cosmic-ray protons this corresponds to a primary energy of ~ 50 TeV, but showers in the threshold range are poorly reconstructed, having an uncertainty in direction of $\sim 3^\circ$ to 4°[5]. The accuracy improves to $\approx 1.5^\circ$ for $S(30) > 5$ (~ 150 TeV for protons and ~ 300 TeV for Fe) and to $\sim 1^\circ$ for showers with energy above 1 PeV. Since many properties of cosmic-ray showers are energy-dependent (as well as the detector response of both SPASE and AMANDA), in what follows we divide the complete set of data and Monte Carlo into four large bins of $S(30)$: $5 < S(30) \leq 10$, $10 < S(30) \leq 25$, $25 < S(30) \leq 50$, and $S(30) > 50$. The lowest-energy bin includes events with energies up to ~ 300 TeV (depending on mass of the primary nucleus), while the highest-energy bin is roughly the region of the knee (1-10 PeV).

High energy muons in the shower core with sufficient energy at production propagate down through the ice and are visible in AMANDA for showers with trajectories within the acceptance cone. The minimum energy of a muon required to reach the top of AMANDA-B10 from SPASE-2 is about 370 GeV, and muons with $E_\mu > 540$ GeV at production can penetrate through it. Since the lateral distribution of the muon bundles is determined primarily from the transverse momentum of the pions at production 10-20 km above the ground, the muon bundles are characterized by a typical radius of ~ 20 m at the top of AMANDA-B10 and ~ 10 m at the bottom. About half the muons that reach the top of AMANDA-B10 range out inside it. In Fig. 3 we show simulated lateral distributions of muons for proton and iron showers at 1730 m depth for the standard four bins of $S(30)$. The intercept gives the average muon multiplicity for each class of events. For a given $S(30)$ showers generated by heavy primaries give more muons than showers generated by protons. There are two reasons for this. First, for the same primary energy, heavy primary nuclei produce more muons because shower pions are more likely to decay than interact (assuming the energy per nucleon is high enough to be outside the threshold region) [16]. Second, for a given $S(30)$ the energy is higher for a heavy nucleus than for protons, as shown in Fig. 2 and by the energy ranges listed on the plots in 3.

Whenever an air shower triggers one of the surface arrays, a trigger window is opened to read out AMANDA. The window is 32 μs in length, and its

delay is adjusted to account for the propagation time of the muons in the air shower core to reach AMANDA and for the signals to propagate back up the AMANDA cables. The total acceptance of SPASE-2–AMANDA-B10 is small. As a consequence, most showers reconstructed by SPASE do not trigger AMANDA. Coincident events occur only when the direction of the air shower at the surface defines a trajectory that extends through or near AMANDA. Coincidences are identified offline by making use of the GPS time tags of the surface and AMANDA events.

2 Angular resolution and pointing of AMANDA-B10

Most, but not all, AMANDA modules face downward, in keeping with its primary function as a neutrino telescope. The detector nevertheless has good sensitivity to downgoing muons, as illustrated by the fact that hit probability for upward and downward facing OMs is similar in air showers observed in coincidence by SPASE and AMANDA. Thus downgoing events can be used to calibrate the response of AMANDA to both downward and upward events. Because air showers that trigger SPASE typically contain several muons with sufficient energy to reach the depth of AMANDA, however, the downgoing coincident events are in a different class from both single downgoing atmospheric muons and neutrino-induced upgoing muons.

A straightforward measure of the angular resolution and pointing accuracy of AMANDA is obtained by comparing the directions assigned by the AMANDA reconstruction algorithm for coincident events with the directions assigned independently to the same events by SPASE. For this analysis we selected a sample of events well-reconstructed in both SPASE and AMANDA. The cuts on the surface parameters are: $S(30) > 5$, shower core within the perimeter of the array, and projected shower core passing inside the AMANDA-B10 cylinder. In AMANDA various quality cuts are used for analysis of neutrino-induced upward muons. An inverted version of these quality cuts was used here for downgoing events. Specifically, we require a sufficiently downgoing fitted zenith angle, a large number of "direct" hits (meaning hits with an arrival time close to the expected arrival time of the Cherenkov cone), a long length of the projection of these direct hits onto the track, a small difference between zenith angles of tracks reconstructed in two different ways, and a sufficiently large velocity of the linefit.

Figure 4 shows the distributions of the angle in space between the direction assigned by the surface air shower arrays and the direction assigned by AMANDA-B10 for coincidences with SPASE-1 and with SPASE-2. As a measure of the width of the distribution of space-angle difference, we use the half-angle of the cone that contains 63% of the events, σ_{63}. The values are 4.4° and

5.2° respectively for SPASE-1 and SPASE-2 coincidences. Given the estimate of $\sigma_{63} \approx 1.5°$ for SPASE, we can estimate the accuracy of AMANDA-B10 for reconstructing direction air shower cores that trigger SPASE and AMANDA as $\sigma^2_{B10} = \sigma^2_{63} - (1.5)^2$, where σ_{63} is obtained from the distributions shown in Fig. 4. This gives $\sigma_{63}(B10) \approx 4.1°$ for events from the direction of SPASE-1 and $\approx 5.0°$ from the direction of SPASE-2.

As in Refs. [17,18], we find, however, that the space-angle distribution is not fit well by a single two-dimensional Gaussian, but requires two components with comparable weights. Such two-component fits are shown here by the curves in Fig. 4. In Ref. [17] the need for two components was traced to degrading of the angular resolution for high-energy muons based on simulations of neutrino-induced muons. The situation here is further complicated by the possibility of multiple muons. The medians of the distributions in Fig. 4 are 3.4° and 3.8° for SPASE-1 and SPASE-2 respectively. These values characterize the distribution of differences in direction between two independent experimental measurements of the same events, one with a surface array, the other with AMANDA-B10. The corresponding median of the difference between true direction and reconstructed direction found in the simulation of Refs. [17,18] is 3.9°. Thus we confirm by an independent analysis the results for resolution used in the AMANDA point source search.[18]

We have also compared the absolute directions assigned by SPASE with those assigned by AMANDA-B10 to see if there is a systematic offset in the absolute pointing. Although there is no significant offset in azimuth, the zenith angle distribution shows a systematic average offset of $\sim 1.5°$, as shown in Fig. 5. To investigate whether this offset may be in part due to the lateral extent of the muon bundles, we can also compare with a sample of smaller showers which generally give single muons at AMANDA. This is possible because the GASP atmospheric Cherenkov telescope [7] was also running during 1997. Because the threshold of GASP for cosmic-ray showers is significantly lower than for the air shower detectors, GASP coincidences consist mostly of single muons at AMANDA. These events therefore have different systematics from SPASE events.

Fig. 5 shows the measurements of absolute pointing relative to the three surface detectors. The two GASP cameras give different offsets. This is not understood, but we note that the two cameras point at different portions of AMANDA [8]. In particular, the camera focussed on events pointed near the top of the instrumented volume of AMANDA-B10 shows the larger offset. The SPASE-1 and SPASE-2 offsets can vary anywhere between 0.8° and 2.2° depending on the cut values required in the AMANDA quality parameters described earlier. GASP, SPASE-1 and SPASE-2 all agree, however, in showing a small systematic offset in zenith of about 1.5° relative to AMANDA. Since GASP shows a similar offset to SPASE, we conclude that the offset is not a

consequence of the spread of the muon bundles. Given the fixed locations of the surface detectors, this experimental check of pointing is only possible for fixed zenith angles. Refs. [17,18] include Monte Carlo studies of the offset that independently confirm the offset obtained from SPASE data and which extend the analysis to all directions for single muons.

The direction of the systematic offset shows that AMANDA tends to assign a smaller zenith angle than the surface detectors. A possible source of this systematic effect is the long, narrow shape of AMANDA-B10 coupled with the errors in the direction as determined by SPASE. Since a thin vertical detector reconstructs vertical events with higher efficiency than oblique ones, the coincidence sample is biased in favor of events in which the true zenith angle is smaller than that assigned by SPASE. The offset is substantially smaller than the angular resolution of AMANDA-B10 and small compared to the size of the point source search bin, which has a half angle $\sim 6^\circ$ [17,18].

3 Muon Tomography

The response of the AMANDA optical modules to muons in cores of air showers can be used to map the deep array and study properties of the ice in which they are embedded.

3.1 Muon survey of AMANDA-B10

Two methods have been used to obtain a muon survey of AMANDA OM locations. Both start from the zenith and azimuth of showers as determined by SPASE for events in which a particular OM in AMANDA-B10 registers a signal. In the first method, we plot the distributions of zenith and of azimuth of all coincident events in which a particular AMANDA OM was hit. This is repeated for each OM. For zenith angle, the distributions obtained in this way are divided by the zenith angle distribution for all SPASE triggers in order to remove the bias associated with the steep zenith-angle distribution convolved with the resolution of SPASE. The fitted mean directions (zenith and azimuth) are determined in this way for each OM. Fig. 6 shows the result for the survey of AMANDA-B10 from SPASE-1 using this method. The fitted directions for each OM are compared to the directions from the center of SPASE-1 as determined from the AMANDA survey.

SPASE-2 is larger and closer to AMANDA than SPASE-1. Thus the approximation underlying the first method (that every trajectory passes through the center of the surface array) introduces relatively larger errors. We therefore

adopted a second survey method in which the expected direction for each event was taken as the direction from the shower core at the surface (as determined by SPASE for the event) to the OM position as determined from the AMANDA survey, which consists of station surveys, drill log data and internal laser calibrations [6]. The apparent direction for a particular event is then the measured direction of the event as determined by SPASE. For each OM the distributions of apparent minus expected angle were fitted for zenith and azimuth separately. For SPASE-1 the results are indistinguishable from Fig. 6. The muon survey of SPASE-2 using this event-by-event method is shown in Fig. 7. The agreement with the nominal OM locations is within $\sim$0.5° in azimuth ($\sim$ 3 m laterally), and there is a 0.5° systematic offset in zenith (bottom panel).

While the event-by-event method is geometrically more accurate, the trigger biases due to the steep zenith angle distribution have not been explicitly removed (though the apparent-minus-expected distributions for each OM are fitted to a Gaussian plus a background which is allowed to have a linear dependence on angle). To study these systematic effects, we performed the same survey with simulated data. The simulations show essentially no offset in azimuth, as expected, while the average 0.5° offset in zenith seen in the data is reproduced. This gives confidence in the absolute positions of both detector components.

3.2 Ice Properties

The same data used for the survey of OMs can be used to obtain a relative measure of attenuation of light in the ice. This is done by comparing the response of OMs at different depths to showers as a function of impact parameter. Absorption of light in the ice is dominated by dust, and modules embedded in layers with more dust cannot see events from as far away as those in clearer layers. Since the impact parameter for each event is determined by projecting the trajectory determined by SPASE, the impact parameter distribution is spread significantly compared to the true distribution. Rather than deconvolving the angular resolution effect here, we simply show that the ice properties revealed by the muons are qualitatively similar to those from laser studies [19].

To do this, we define a parameter λ which is determined by fitting the distribution of hit probabilities for each OM to an exponential distribution as a function of apparent impact parameter. In this way, a value of λ is determined for each OM. Fig. 8 shows λ as a function of depth. The prominent features of this plot match up well in depth with variations in the optical properties of south pole ice as determined from completely independent methods. In

Ref. [19], the scattering coefficient of ice as a function of depth was obtained by fitting arrival time distributions of pulsed light sources sent and received between AMANDA OMs at various separations but similar depths. Depths of minimum and maximum scattering found in that analysis correspond closely to maxima and minima respectively in Fig. 8, as expected since scattering is proportional to $1/\lambda$.

4 Muon bundles in AMANDA

In [1] we use the muon bundles seen by AMANDA in coincidence with air showers measured by SPASE for a study of primary cosmic-ray composition. To do this we need to measure the lateral distribution of the light generated by the muons in AMANDA, which requires knowing the trajectory of each coincident event as accurately as possible. Rather than using the trajectory determined by SPASE alone or by AMANDA alone, we fix the location of the trajectory to coincide with the core location at the surface as measured by SPASE. Then the direction is determined with the AMANDA reconstruction program subject to this constraint. Fig. 9 shows examples of the measured lateral distributions of pulse heights from light generated by six large muon bundles in AMANDA for which the trajectories were determined in this way. The well-determined lateral distribution of the muon light pool measured by AMANDA demonstrates that the combined track fit works and that the light pool produced by a muon bundle in AMANDA can be measured well. Such measurements form the basis of the composition analysis in [1].

References

[1] K. Rawlins for the SPASE and AMANDA Collaborations, Proc. 28th Int. Cosmic Ray Conf. (ed. T. Kajita *et al.*, Universal Academy Press, 2003) vol. 1, p. 173. (Expanded version to be submitted for publication.)

[2] N.J.T. Smith *et al.*, Nucl. Instr. and Meth. A 276 (1989) 622.

[3] J. Beaman *et al.*, Phys. Rev. D48 (1993) 4495.

[4] J. van Stekelenborg, *et al.*, Phys. Rev. D48 (1993) 4504.

[5] J.E. Dickinson *et al.*, Nucl. Instr. and Meth. A 440 (2000) 95.

[6] The AMANDA Collaboration, E. Andres *et al.*, Astroparticle Physics 13 (2000) 1.

[7] G. Barbagli *et al.* Nucl. Phys. (Proc. Suppl.) 32 (1993) 156.

[8] P. Romenesko, A. Karle, and B. Morse. AMANDA Internal Report 20000905 (2000).

[9] A. Walker *et al.*, Nucl. Instr. and Meth. A 301 (1991) 574.

[10] A.M. Hillas, Proc. 24th Int. Cosmic Ray Conf. **1** (1981) 270, Rome, Italy.

[11] N.N. Kalmykov, S. Ostapchenko, and A.I. Pavlov, Nucl. Phys. B (Proc. Suppl.) **52B** (1997) 17.

[12] J.E. Dickinson *et al.*, Proc. 16th Int. Cosmic Ray Conf. (Salt Lake City) vol. 3, p. 136 (1999)

[13] T. Antoni *et al.*, J.Phys. **G25** (1999) 2161

[14] W. Lohmann, R. Kopp, R. Voss, CERN-85-03; R. Kopp, W. Lohmann, R. Voss, MUDEDX: Parametrization and Monte Carlo generation of energy loss of high energy muons, Version 2.02, 1995, private communication.

[15] S. Hundertmark, Ph.D. Thesis, Humboldt-Universität, Berlin (1999), available at http://amanda.berkeley.edu/manuscripts/.

[16] T.K. Gaisser & Todor Stanev, Nucl. Instruments & Methods A 235 (1985) 183.

[17] S. Young, Ph.D. thesis, University of California, Irvine, 2001.

[18] J. Ahrens *et al.* Astrophys. J. **583** (2003) 1040-1057.

[19] P. B. Price, K. Woschnagg, and D. Chirkin, Geophys. Res. Lett. **27** (2000) 2129.

[20] K. Rochester, Ph.D. Thesis, University of Leeds, 2000.

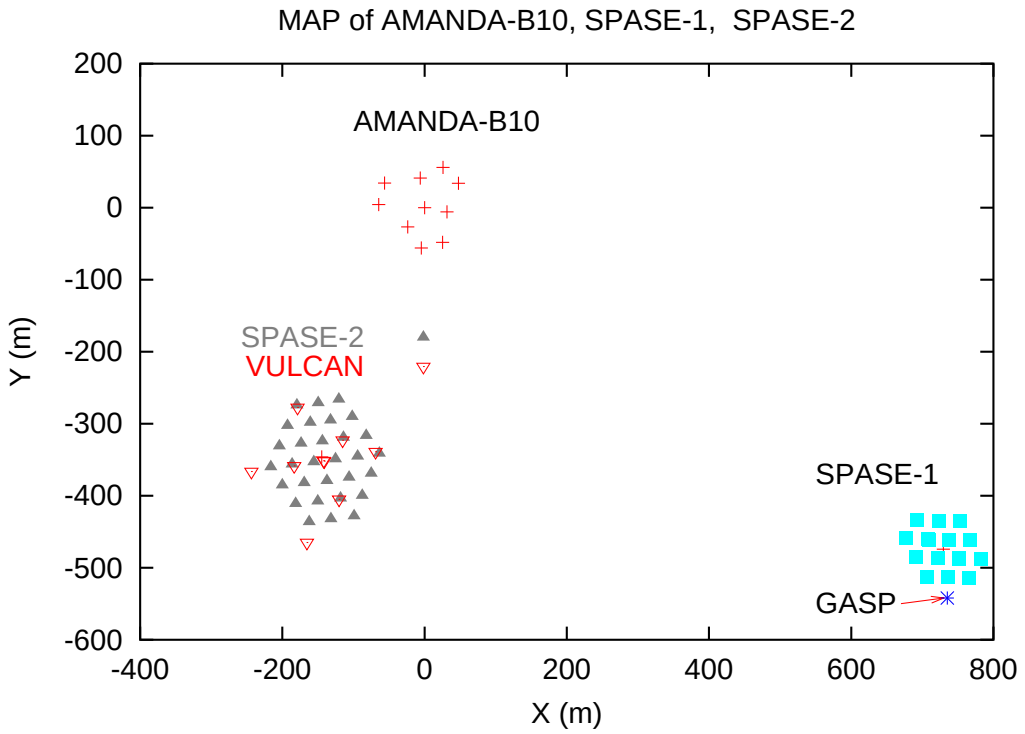

Fig. 1. Map showing locations of SPASE-1 and SPASE-2 relative to locations of AMANDA-B10 strings at the surface. The origin of the local coordinate system for each SPASE array is marked with a red cross. The origin of the AMANDA coordinate system coincides with string 4, and the positive y axis is grid north. Azimuth is measured counter-clockwise from grid east. Thus the center of SPASE-2 is at 247° and the center of SPASE-1 at 327°.

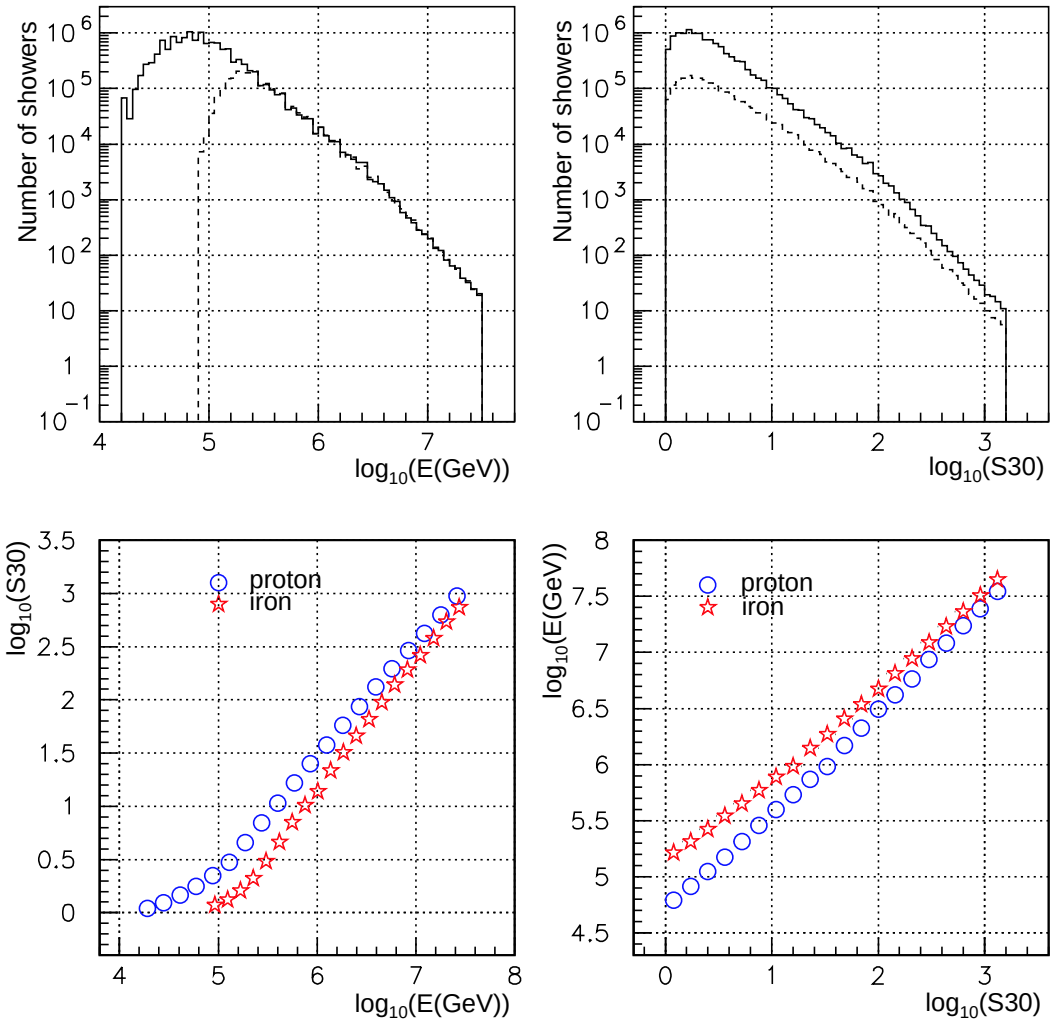

Fig. 2. Distributions of primary energy and $S(30)$ (upper panels), and relationships between them (lower panels), for protons (solid, open circles) and iron (dashed, stars) simulation. The lower panels show $\langle log_{10}(S(30))\rangle$ vs logarithm of energy (left) and $\langle log_{10}(E)\rangle$ vs logarithm of $S(30)$ (right).

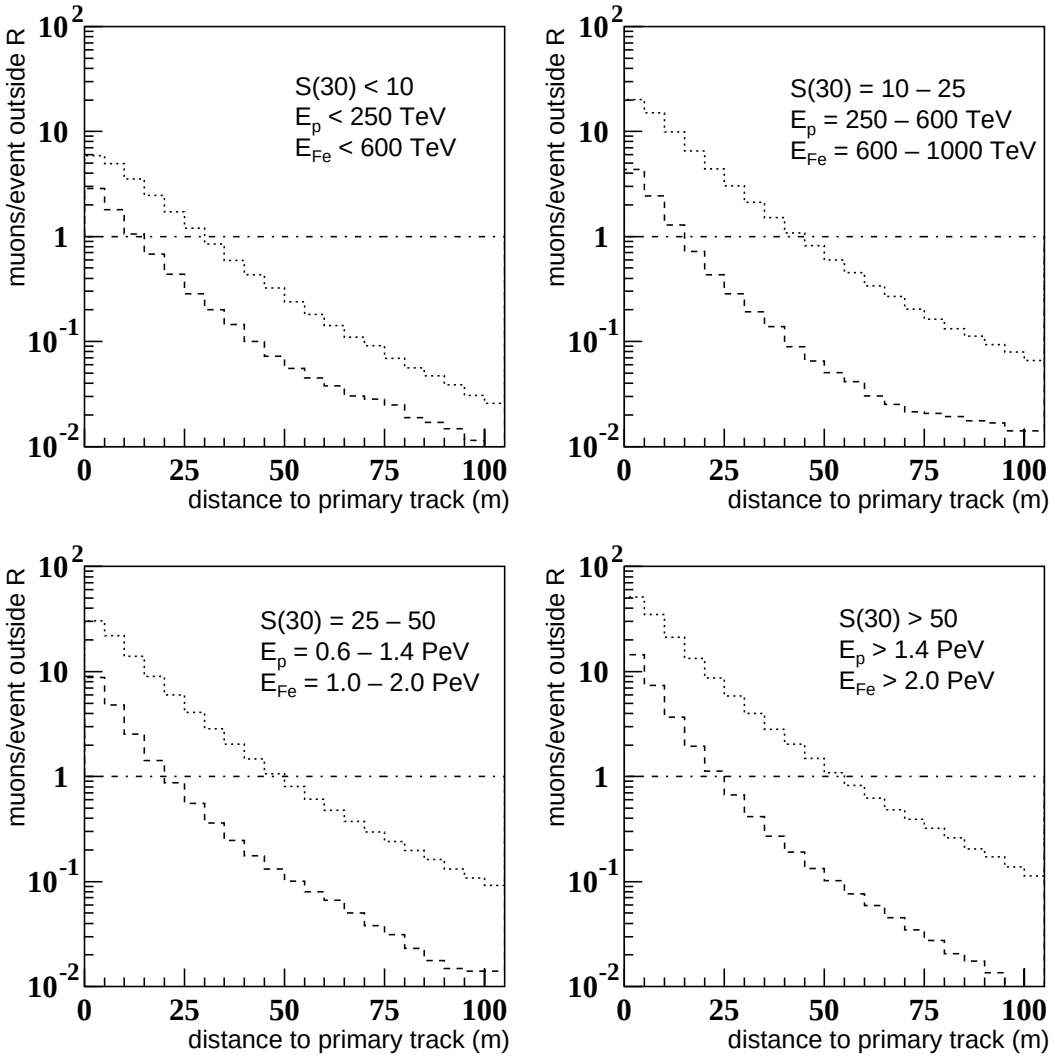

Fig. 3. Integral lateral distribution of muons at the depth of AMANDA for simulated proton (dashed) and iron (dotted) showers. The plot shows the average number of muons at distances larger than a given radius for the four $S(30)$ intervals described in the text. The intercept at zero radius is the average muon multiplicity for the each class of events. Where the histograms meet the horizontal line marks the distance beyond which there is on average less than one muon.

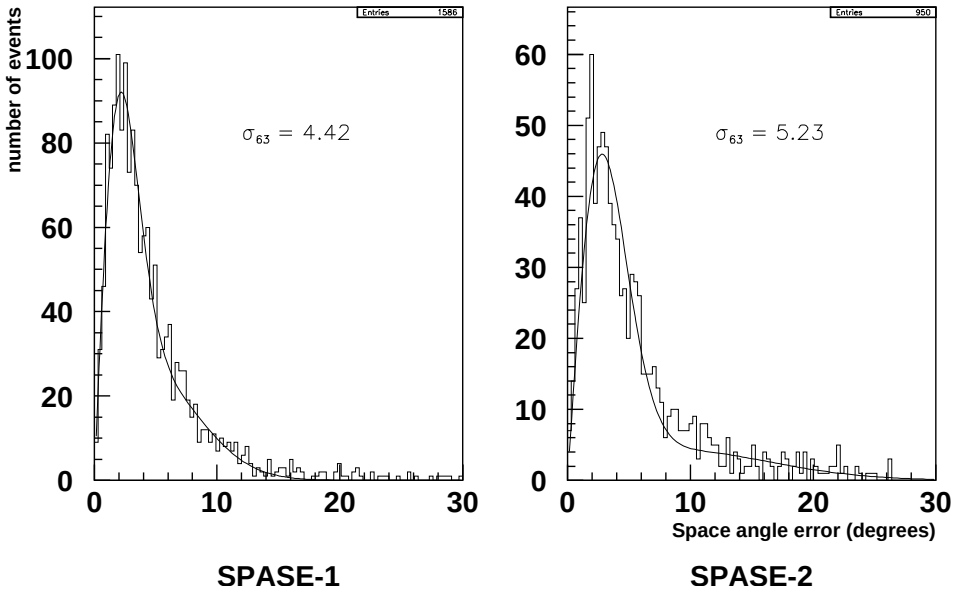

Fig. 4. Distribution of difference between direction assigned by SPASE and that assigned by AMANDA-B10 for a sample of coincident events, fit by a double-Gaussian.

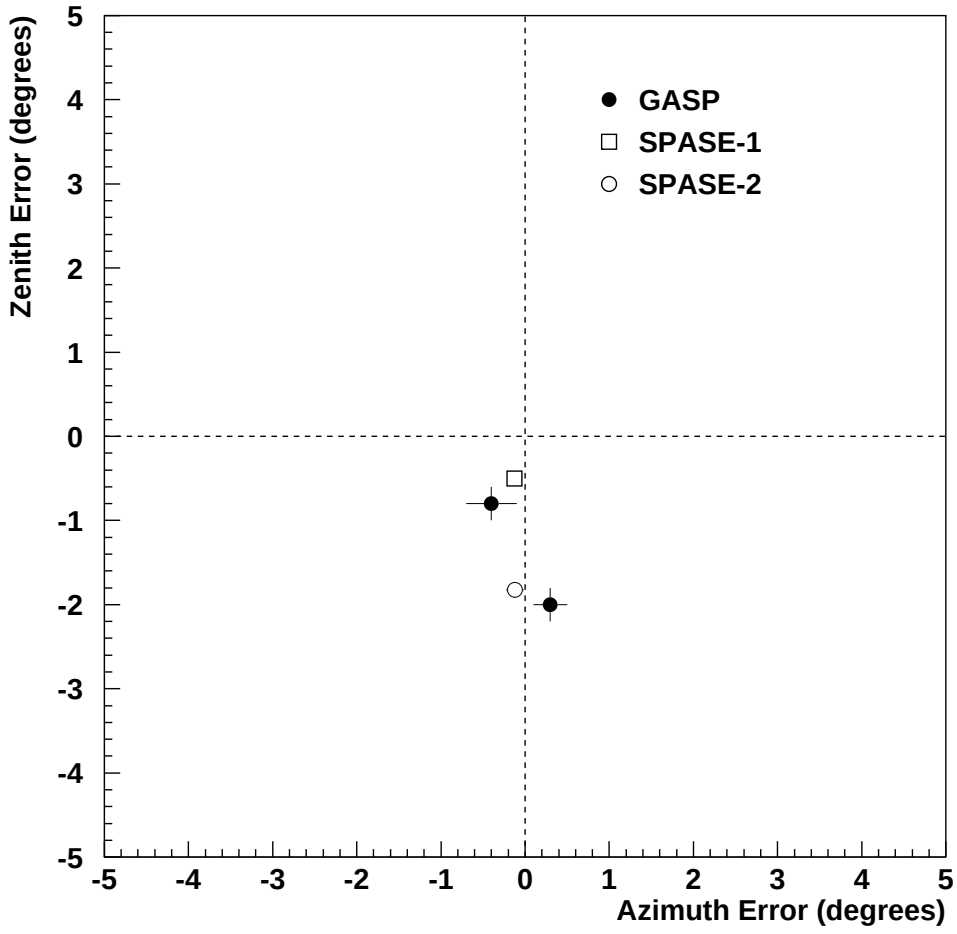

Fig. 5. Three independent measurements of absolute pointing accuracy (origin = perfect pointing). Gasp results from [7] shown separately for two Gasp cameras.

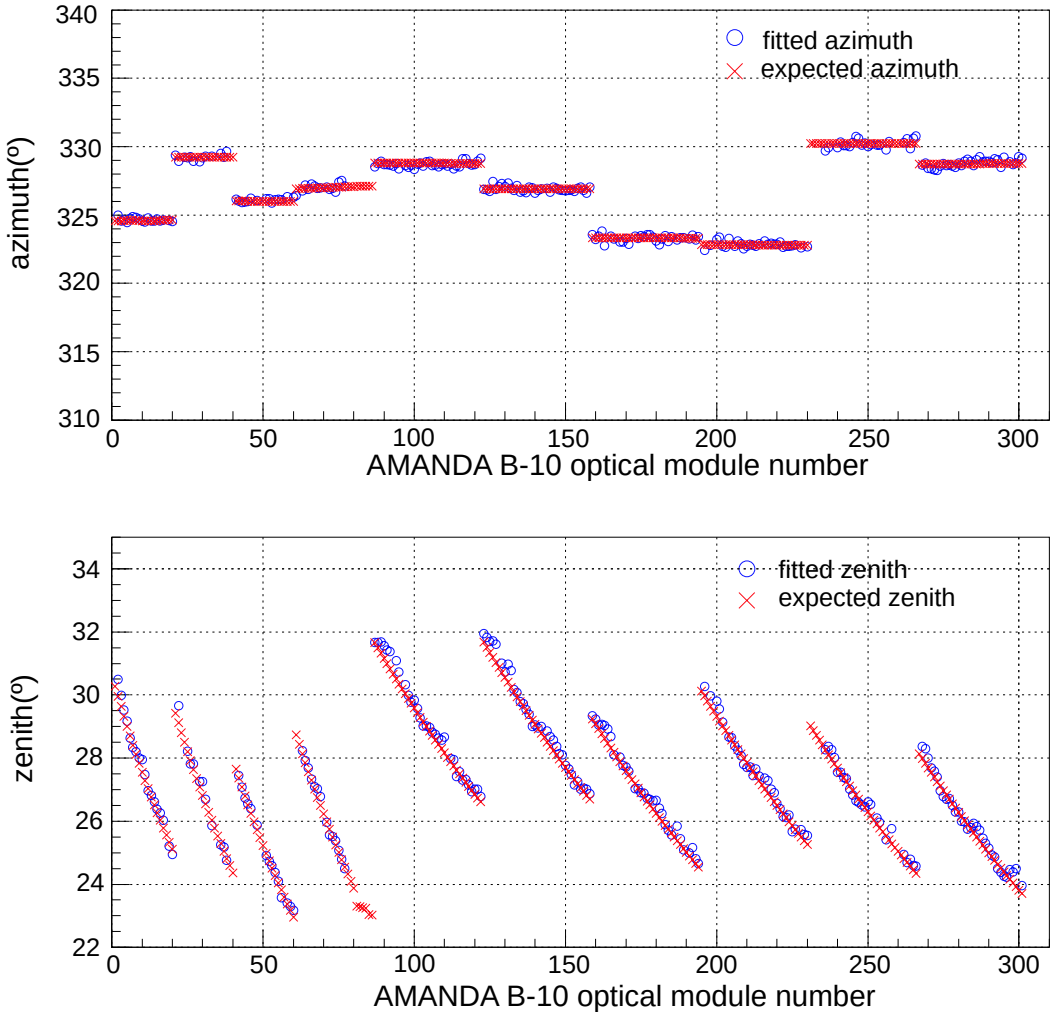

Fig. 6. Muon survey of AMANDA B10 (view from SPASE-1).

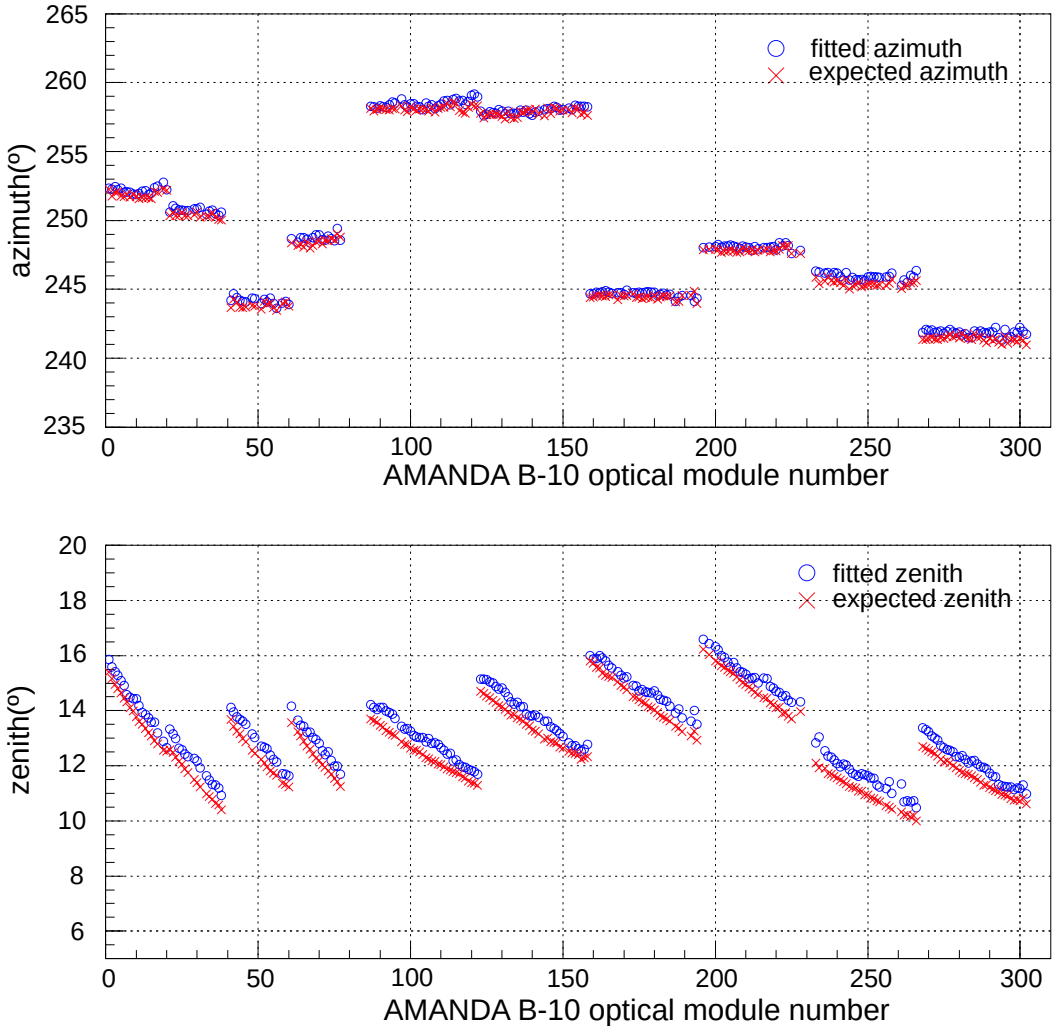

Fig. 7. Muon survey of AMANDA B10 (view from SPASE-2).

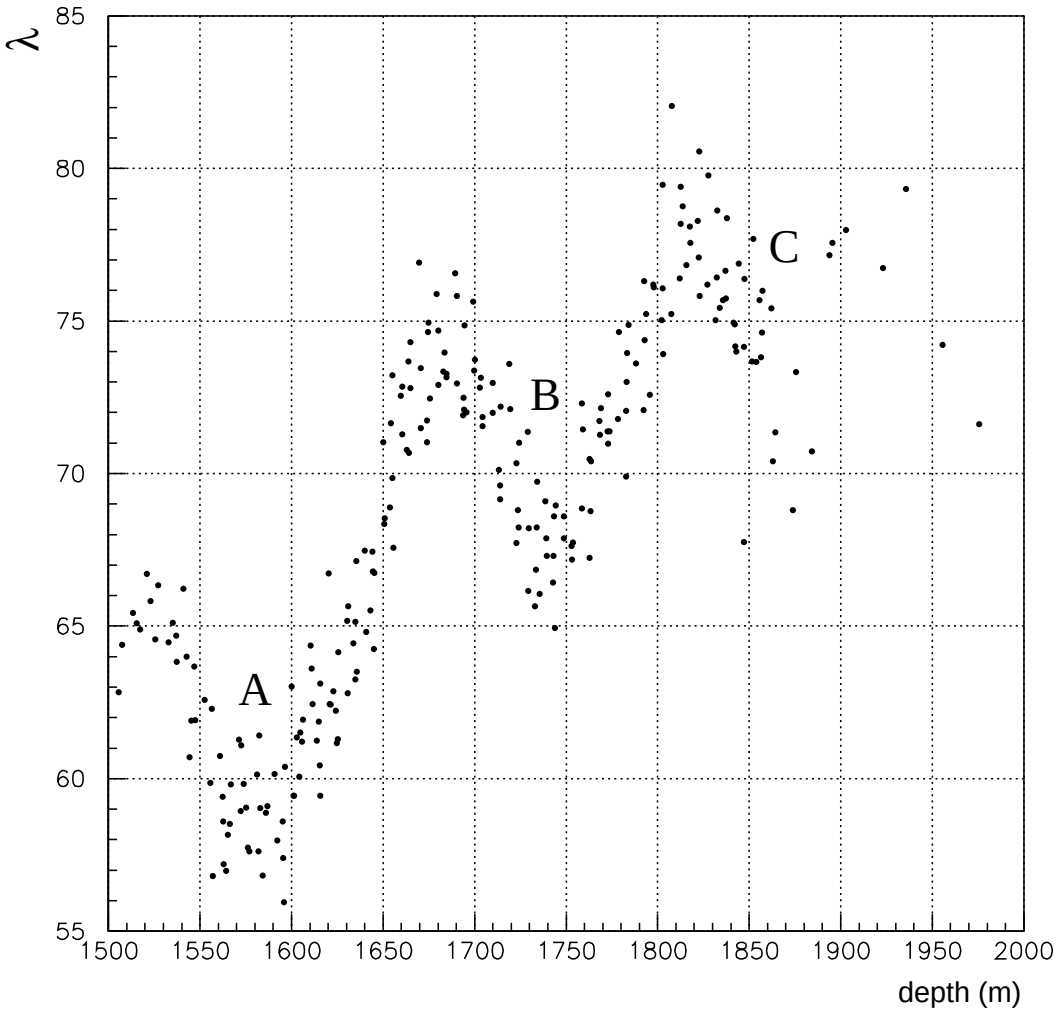

Fig. 8. A simple exponential fit to hit probability as a function of apparent impact parameter reflects the varying ice clarity as a function of depth. See text for a definition of λ. The points A, B and C indicate locations of dust layers described in Ref. [19].

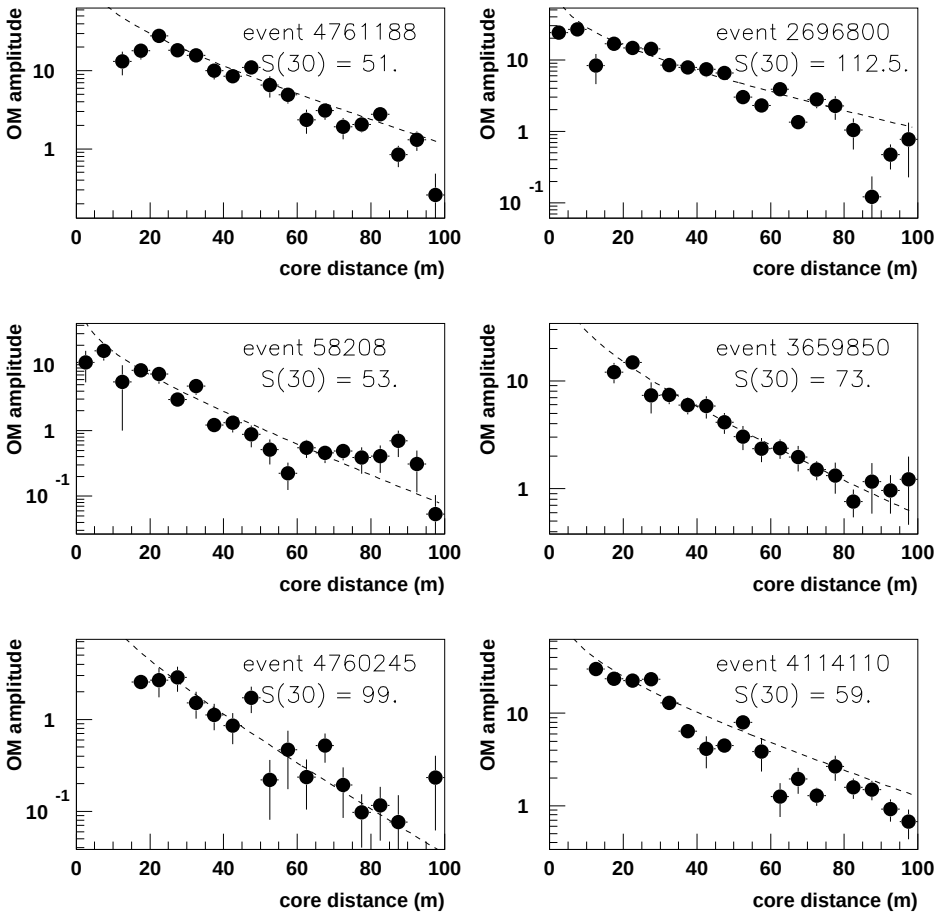

Fig. 9. Lateral distribution of the Cherenkov light signal generated by six muon bundles at AMANDA. Core distance is the perpendicular distance of each OM from the trajectory of the shower core. From the plot of E vs S(30) in Fig. 2, the corresponding estimates of primary energy for these events are in the range 1 to 10 PeV.